Real-time Video Transmission Using Massive MIMO in an Underwater Acoustic Channel

Mohammud J. Bocus, Dimitris Agrafiotis and Angela Doufexi
Department of Electrical and Electronic Engineering, University of Bristol, BS8 1UB, UK.

***Abstract*—In this paper we propose to use massive multiple-input multiple-output (MIMO) systems in order to boost the throughput over a 1000 m vertically-configured time-varying underwater acoustic channel (UAC). We compare the bit error rate (BER) performance of un-coded and Turbo-coded massive MIMO systems based on filter bank multicarrier (FBMC) modulation and Orthogonal Frequency Division Multiplexing (OFDM). A modified FBMC system is considered whereby complex data symbols are transmitted instead of real-valued ones. This is made possible by spreading the data symbols in time while still ensuring maximum bandwidth efficiency and low complexity. It is shown that the coded FBMC systems outperform the coded OFDM systems both in terms of error performance and bit rate for similar massive MIMO configuration. Video transmission is evaluated over the UAC with the systems that achieve the highest bit rates and it is shown that real-time transmission is possible with acceptable video quality over the long range acoustic link.**

I. Introduction

Applications which require real-time and high quality video transmission represents a serious challenge since the acoustic bandwidth is extremely limited, lower bound by noise and upper bound by attenuation. Hence bandwidth-efficient systems need to be used and the negative effects of the UAC should be minimized. In this regard OFDM has been widely investigated for underwater acoustic (UWA) communication. Some studies which considered horizontal transmission have shown that acceptable bit rates can be achieved using single-input single-output (SISO) OFDM, promoting real-time video transmission over a specific range with acceptable quality (e.g., [1], [2]). MIMO-OFDM has also been widely investigated for UWA communication in order to enhance the data rate (e.g., [3]) or improve the reliability of the communication system (e.g., [4]). The problem of using OFDM for UWA communication is that a long cyclic prefix (CP) duration is required to cope with the extended channel impulse response (CIR), especially in shallow water horizontally-configured UACs. Consequently, the OFDM symbol duration should be made longer to maintain a good bandwidth efficiency [5]. However, in fast time-varying UACs, there is too much variation across a symbol, thereby increasing the Doppler-induced inter-carrier interference (ICI) [5]. FBMC has been proposed to address the doubly-dispersive UACs and at the same time increase the achievable bit rate (e.g., [6]–[8]).

Massive MIMO technology is currently being considered for the 5G terrestrial wireless communication systems in order to provide additional data capacity and improve the signal quality. Recently, this technology is also being investigated for UWA communication in order to further enhance the bandwidth efficiency. For instance in [5], an FBMC-based multi-user massive MIMO system with 32 subcarriers is proposed with 4 transmitting stations and 40 receiving hydrophones at the base-station. The system's bandwidth is 5 kHz and the carrier frequency is 8 kHz. Each of the four transmitting stations is equipped with a single loudspeaker. Cosine Modulated Multi-tone (CMT) is selected as the FBMC system. The short symbol duration allowed tracking of channel variations using a blind equalization method based on constant modulus algorithm (CMA). Hence pilot symbols were not used, thereby achieving a high bandwidth efficiency (8 b/s/Hz). A matched filter estimator was used at the receiver. The self-equalisation property of the massive MIMO system allowed 32 wide subcarriers to be used for a system's bandwidth of 5 kHz and carrier frequency of 8 kHz. Simulation results showed that the blind tracking algorithm allowed data to be transmitted without the need for pilot symbols. Furthermore, the signal-to-interference-plus-noise ratio (SINR) for the four users increased from approximately 12 dB to 18 dB with increasing number of base-station hydrophones (from 20 to 100). The authors of [9] derived a closed-form expression for the uplink achievable rate in a massive MIMO-OFDM system with carrier aggregation (CA). Zero-forcing (ZF) equalization was assumed. A synthetic UAC was considered, with a water depth of 5000 m and a fixed receiver array depth of 5 m. The distance between the transmitter (4 transducers) and receiver (100 hydrophones) was varied from 1 km to 25 km in the simulations. A system bandwidth of 20.48 kHz is considered with 2048 subcarriers and a CP duration of 20 ms was assumed. A frequency range from 10 to 500 kHz was allocated for the uplink transmission. Simulated capacity curves showed that the CA massive MIMO system can offer very high data rates (in the order of several Mbps) for both short/medium and long distances compared to systems without CA.

In this work, we consider massive-MIMO reception whereby we have a large array of 100 receiving hydrophones at a surface vessel while a remotely operated underwater vehicle (ROV) is equipped with at most 4 transducers. We examine the bit error rate (BER) performance comparison between uncoded and coded massive MIMO-OFDM and FBMC in a 1000 m

vertically-configured time-varying channel. Offset Quadrature Amplitude Modulation (OQAM) is chosen as the FBMC system since it achieves maximum bandwidth efficiency. A modified FBMC/OQAM system as proposed in [10] is considered whereby complex data symbols are transmitted instead of real symbols. Scattered pilot-based channel estimation is applied to both the massive MIMO-OFDM and FBMC/OQAM systems. The transmission of a 480p video which is compressed using the H.264 Advanced Video Coding (AVC) standard is evaluated in the UAC with the systems that achieve the highest bit rates.

The rest of the paper is organized as follows: The characteristics of an UAC are briefly described in Section II. The discrete-time baseband model for the modified FBMC/OQAM system is presented in Section III. Section IV presents the performance evaluation of the systems in the vertically configured UAC. Finally, conclusions are given at the end of this paper.

Notation. The complex conjugate of x is given as x^*. The superscripts $^{\mathrm{T}}$ and $^{\mathrm{H}}$ denote the transpose and Hermitian transpose operations respectively. $\mathbf{I}$ is an identity matrix.

II. Underwater Acoustic Channel

A. Path Loss

High frequency acoustic signals are more attenuated than low frequency ones for a given distance. The path loss in terms of a transmission distance x and signal frequency f is given by [11]

$$A(x,f) = x^k \alpha(f)^x, \tag{1}$$

where k is the geometrical spreading factor taking values of 1 and 2 for shallow and deep water respectively and $\alpha(f)$ is the absorption coefficient which can be computed in dB/km for f in kHz using the Thorp's formula as follows [12]

$$10\log\alpha(f) = \frac{0.11f^2}{1+f^2}+\frac{44f^2}{4100+f^2}+2.75\times10^{-4}f^2+0.003. \tag{2}$$

B. Propagation Delay

The speed of sound (v) in water is given by [12]

$$\begin{aligned} v &= 1448.96+4.591\theta-0.05304\theta^2+0.00023 74\theta^3 \\ &+ 1.340(S-35)+0.0163z+1.675\times10^{-7}z^2 \\ &- 0.01025\theta(S-35)-7.139\times10^{-13}\theta z^3, \end{aligned} \tag{3}$$

where z is the water depth between 0 and 8000 m, S is the salinity between 30 and 40 parts per million (ppm) and θ is the water temperature between 0 and 30^{o}C. Sound propagates very slowly underwater ($\approx$ 1500 m/s) and when the transmission is performed horizontally (direction of the acoustic wave with respect to the sea floor), multipath distortion can be extreme, causing the delay spread to span over tens or even hundreds of milliseconds [13].

C. Ambient Noise

Ambient noise (colored noise) is defined by the Empirical formulas as follows (in dB re μPa per Hz where f is in kHz) [11]

$$\begin{aligned} 10\log N_{tb}(f) &= 17-30\log(f) \\ 10\log N_s(f) &= 40+20(s-0.5)+26\log(f)- \\ &\quad 60\log(f+0.03) \\ 10\log N_w(f) &= 50+7.5w^{0.5}+20\log(f)-40\log(f+0.4) \\ 10\log N_{th}(f) &= -15+20\log(f), \end{aligned} \tag{4}$$

where N_{tb} is the turbulence noise, N_s is the shipping noise (s is known as the shipping factor taking values between 0 and 1), N_w is the noise caused by breaking waves as a result of wind (w is the wind speed in m/s) and N_{th} is the thermal noise. Considering all the noise sources, the overall power spectral density (PSD) of ambient noise is given by (in μPa) [11]:

$$N_{all}(f) = N_{tb}(f)+N_s(f)+N_w(f)+N_{th}(f). \tag{5}$$

D. Signal-to-Noise Ratio (SNR)

The SNR (in μPa re dB per Hz) in an UAC is expressed as follows [11]

$$SNR(x,f) = \frac{S_{tx}(f)}{A(x,f)N_{all}(f)}, \tag{6}$$

where $S_{tx}(f)$ is the transmitted signal PSD whose power can be adjusted according to a given transmission distance [13]. The narrowband SNR is thus a function of frequency and for each transmission distance, there is an optimum frequency at which the SNR is maximum.

E. Multipath

In a multipath channel, the frequency response of the rth path is given by [14]

$$H_r(f) = \Gamma_r/\sqrt{A(x_r,f)}, \tag{7}$$

where x_r is the length of the rth path with a delay of $\tau_r=(x_r/v)-t_0$ (t_0 is a reference time at the receiver), Γ_r is the cumulative reflection coefficient due to the surface and bottom reflections. The surface reflection coefficient equals to -1 under ideal conditions while the bottom reflection coefficients depend on the hardness or softness of the sea floor as well as the grazing angle [13]. The overall channel frequency response (CFR) is expressed as [14]

$$H(f) = \sum_r H_r(f)e^{-j2\pi f\tau_r}, \tag{8}$$

and the corresponding impulse response is given by

$$h(t) = \sum_r h_r(t-\tau_r), \tag{9}$$

where $h_r(t)$ is the inverse Fourier transform of $H_r(f)$.

Motion of the transmitter and/or receiver causes an extreme Doppler effect in an UAC, the magnitude of which is proportional to the ratio $\xi=v_{txrx}/v$ [13]. ξ is known as the Doppler scale factor and v_{txrx} is the relative velocity between the transmitter/receiver pair. Autonomous underwater vehicles (AUVs) usually move at speeds in the order of a few m/s, but

even when stationary, unintentional motion can occur due to ocean currents or tides. The low speed of sound underwater makes motion-induced Doppler distortion non-negligible as compared to a highly mobile terrestrial radio system where ξ can be as low as 10^{-7} [13]. A time-varying UAC can be expressed as [11]

$$h(\tau,t) = \sum_{r}\Omega_r(t)\delta(\tau-\tau_r(t)), \tag{10}$$

where $\Omega_r(t)$ is the time-varying amplitude of the rth path. It is assumed that the paths amplitudes are constant within a short data block such that $\Omega_r(t)\approx\Omega_r$. Considering N_{pa} discrete paths, a Doppler scale factor ξ can be applied to each path delay and hence (10) can be re-written as follows [11]

$$h(\tau,t)=\sum_{r=1}^{N_{pa}}\Omega_r\delta(\tau-[\tau_r-\xi_r t]). \tag{11}$$

III. System Model

A. FBMC/OQAM

In a conventional FBMC/OQAM system, real symbols are transmitted allowing prototype filters with good time/frequency localization (TFL) property to be used. While FBMC/OQAM achieves a maximum bandwidth efficiency of $TF=1$ (where T and F are the time and subcarrier spacings respectively), its orthogonality condition only holds in the real field. The objective is to design a prototype filter which exhibits complex orthogonality for $TF=2$ (such as a Hermite filter). So both the time and frequency spacings are reduced by a factor of 2 such that $TF=0.5$ (real symbols) which is equivalent to $TF=1$ (complex symbols) in terms of transmitted data per timing instance [10]. This compression in time and frequency causes purely imaginary interference (due to a phase shift) which makes channel estimation and application to MIMO challenging. The authors of [10] proposed to spread the symbols either in time or frequency to completely eliminate the imaginary interference. This process not only allows complex symbols to be transmitted but also ensures a low complexity since it is based on Hadamard matrices. For an FBMC/OQAM system with M subcarriers and N symbols, the transmitted signal $s(t)$ can be expressed as [10]

$$s(t)=\sum_{n=1}^{N}\sum_{m=1}^{M}g_{m,n}(t)d_{m,n}, \tag{12}$$

where $d_{m,n}$ are the transmitted symbols on the mth subcarrier at the nth timing instant. $g_{m,n}(t)$ is a time/frequency shifted version of a prototype filter $p(t)$ which is given by

$$g_{m,n}(t)=p(t-nT)e^{j2\pi mF(t-nT)}e^{j\theta_{m,n}}, \tag{13}$$

where $\theta_{m,n}=\frac{\pi}{2}(m+n)$ is the phase shift. The received symbols $y_{m,n}$ are obtained by projecting the received signal $r(t)$ on $g_{m,n}(t)$ as follows [10]

$$y_{m,n}=\langle r(t),g_{m,n}(t)\rangle=\int_{-\infty}^{\infty}r(t)g^{*}_{m,n}(t)\mathrm{d}t, \tag{14}$$

Formulating (12) in matrix notation yields the following

$$\mathbf{s}=\mathbf{G}\mathbf{d}, \tag{15}$$

where the column vectors of $\mathbf{G}$ represent the basis pulses $g_{m,n}(t)$ in matrix notation and $\mathbf{d}$ is the transmitted symbol vector which is represented as follows

$$\mathbf{d}=\begin{bmatrix}d_{1,1} & d_{2,1}\cdots d_{M,1} & d_{1,2}\cdots d_{M,N}\end{bmatrix}^{\mathrm{T}}. \tag{16}$$

The received signal vector can be written as

$$\begin{aligned}\mathbf{y}&=\mathbf{T_{mat}}\mathbf{d}+\boldsymbol{\eta}\\&=\begin{bmatrix}y_{1,1} & y_{2,1}\cdots y_{M,1} & y_{1,2}\cdots y_{M,N}\end{bmatrix}^{\mathrm{T}},\end{aligned} \tag{17}$$

where $\boldsymbol{\eta}$ is the random noise vector and $\mathbf{T_{mat}}$ is the transmission matrix which is defined as follows

$$\mathbf{T_{mat}}=\mathbf{G}^{\mathrm{H}}\mathbf{G}. \tag{18}$$

While $\mathbf{T_{mat}}$ is an identity matrix in OFDM, it is not in FBMC due to the interference from the imaginary components [10]. In order to obtain an identity matrix, only the real part of the transmission matrix needs to be considered, i.e., $\mathcal{R}\{\mathbf{T_{mat}}\}=\mathbf{I_{MN}}$. When $\{M,N\}\rightarrow\infty$, $\mathbf{T_{mat}}$ contains exactly $\frac{MN}{2}$ non-zero eigenvalues, each having a value of two [10]. This means that only $\frac{MN}{2}$ complex symbols can be transmitted (or equivalently MN real symbols).

B. Modified FBMC/OQAM

The uncorrelated data symbols, denoted as $\tilde{\mathbf{d}}$, are precoded using a unitary coding matrix $\mathbf{C}$ such that the transmitted symbols are given by [10]

$$\mathbf{d}=\mathbf{C}\tilde{\mathbf{d}}. \tag{19}$$

In order to eliminate the imaginary interference, the coding matrix should satisfy the following condition [10]

$$\mathbf{C^{H}T_{mat}C}=\mathbf{I}. \tag{20}$$

At the receiver, decoding is performed such that the received data symbols are obtained as follows

$$\tilde{\mathbf{y}}=\mathbf{C^{H}}\mathbf{y}. \tag{21}$$

$\frac{N}{2}$ appropriate column vectors are extracted from a Hadamard matrix of order N which are then used to spread the complex symbols over several time slots. The process is done for all subcarriers until a coding matrix of size $MN\times\frac{MN}{2}$ that satisfies the condition in (20) is obtained.

IV. Performance Evaluation

A. BER Performance

A near-vertical channel with a water depth of 1000 m is considered. The transmitter and receiver are immersed at a depth of 998 m and 1 m respectively. The horizontal separation between them is assumed to be 5 m. The system's bandwidth is set at 25 kHz and the carrier frequency f_c is 32.5 kHz. The channel coefficients are generated using a statistical model based on the maximum entropy principle [15]. It is assumed that there is a relative speed of 2 m/s between the transmitter/receiver pair, resulting in a maximum Doppler frequency

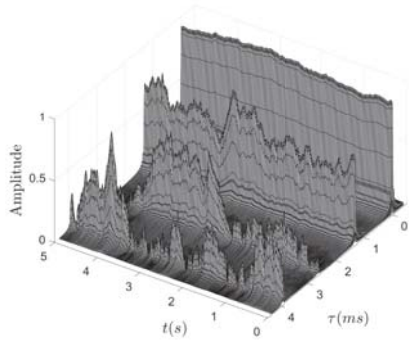

(a)

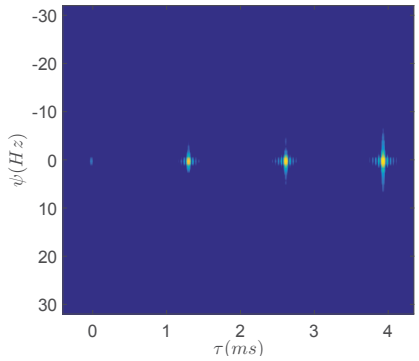

(b)

Fig. 1. Vertical Channel (a) CIR (b) CSF

of approximately 43.3 Hz. The Doppler spread is assumed to increase linearly from 0.5 Hz to 2 Hz with each channel tap delay. The channel impulse response (CIR) and channel scattering function (CSF) are shown in Fig. 1. The maximum delay spread in the UAC is 3.9 ms. The CSF characterizes the average output power in the channel as a function of the delay τ and Doppler ψ. In other words, it gives an indication of the rate of channel variations at different multipath delays. The number of subcarriers is set at 256 for both the FBMC and OFDM systems. Colored noise is also used in the simulations instead of additive white Gaussian noise (AWGN) to better represent the real-world UWA scenario. The other system parameters include 64-QAM modulation and 1/2-rate Turbo code for the coded MIMO systems (with N_t transmitters and N_r receivers). Due to the time spreading, block-wise transmission is considered with 64 FBMC symbols (real) and a zero time-slot per block (to minimize interblock interference). With time spreading, we have 32 complex symbols per subcarrier per block for the FBMC system. Considering a CP duration of 5.12 ms and assuming the same transmission time as in the FBMC system, the OFDM system will require 22 complex symbols per subcarrier per block. No guard slot is required between blocks for the OFDM case. Pilot-based channel estimation is considered for both the OFDM and FBMC/OQAM systems with the pilots arranged as in Long-Term Evolution (LTE).

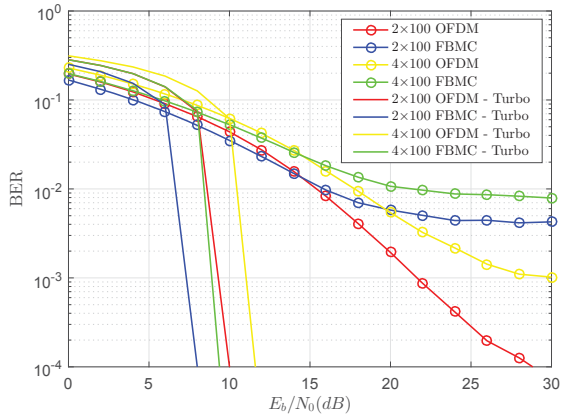

Fig. 2. BER performance of OFDM & FBMC/OQAM with massive MIMO reception in a 1000 m vertical UAC

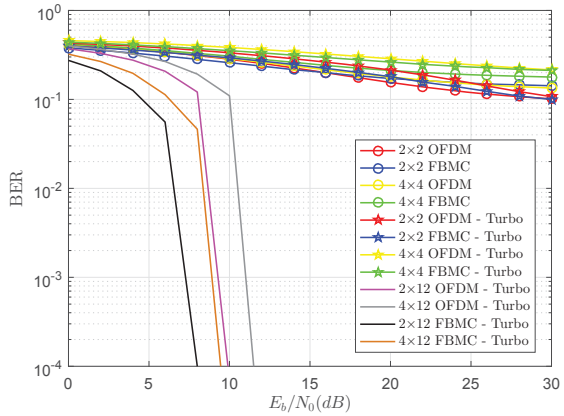

Fig. 3. BER performance of standard MIMO-OFDM & FBMC/OQAM systems in a 1000 m vertical UAC

For similar transmission time, the FBMC and OFDM systems transmit 340 pilots and 255 pilots respectively per hydrophone. In order to prevent interference, at the pilot positions of one transmitting hydrophone, the other hydrophones should transmit zero symbols. A large receiver array of 100 hydrophones is assumed. In order to ensure decorrelated received signals, the inter-element spacing must be greater than at least half a wavelength [16], which in our case is equal to 2.3 cm (assuming a sound velocity of 1500 m/s).

The BER performance for massive MIMO OFDM and FBMC/OQAM systems in the vertical UAC is shown in Fig. 2. The receiver processing consists of least-square (LS) channel estimation with linear interpolation and zero-forcing (ZF) equalization. A Hermite filter with an overlapping factor of 4 is considered for the FBMC system. At high E_b/N_0 values, the performance of the un-coded massive MIMO-OFDM systems is better. In theory, the number of FBMC symbols can approach infinity but due to the time spreading over N time slots, this is not practical because of latency limitation and the time-varying nature of the channel with destroys orthogonality. This is why block-wise transmission is considered. The blocks slightly overlap and in a conventional

TABLE I
THEORETICAL ACHIEVABLE BIT RATE (kbps)

System Configuration	OFDM	FBMC/OQAM
2×12	40	59
4×12	73	108
2×100	91	133
4×100	164	242

FBMC system, this overlapping is not a problem due to the real orthogonality condition. However, this is no longer valid if time spreading is applied within a transmission block [10]. One guard slot per block may not completely eliminate the interference between neighboring blocks. On the other hand using more guard slots will decrease the spectral efficiency. By using a higher spreading length in a time-invariant channel, the interference can be spread over a higher number of symbols, thereby improving the signal-to-interference (SIR) [10]. For a time-varying channel, the robustness of the systems can be increased using a smaller spreading length [10]. Considering the 1/2-rate Turbo coded systems, the 2×100 and 4×100 FBMC/OQAM systems outperform the OFDM systems with similar configuration by 2 dB and 2.2 dB respectively at a BER of 10^{-4}. For comparison purposes, the BER performance for standard symmetric MIMO configurations (2×2 and 4×4) in the same channel is shown in Fig. 3. The parameters are similar to the massive MIMO systems. Even with the use of Turbo codes, the 2×2 and 4×4 FBMC and OFDM systems achieve a high error rate. The application of massive MIMO reception to the OFDM and FBMC/OQAM systems greatly improve the BER performance for similar system parameters. Usually for UWA communication, asymmetric MIMO configuration is used where N_r>N_t (e.g., [16]). Hence, coded 2×12 and 4×12 MIMO systems are included in Fig. 3. In order to achieve comparable performance as the coded massive MIMO systems in Fig. 2, a lower modulation order (16-QAM) and a lower FEC code rate (1/3) were used for these systems. Hence, the achievable bit rates will be much lower than with the massive MIMO systems.

B. Theoretical Achievable Bit Rate

The same system parameters as used for the simulations are considered for the bit rate computation. The zero guard slots which are inserted between blocks in the modified FBMC/OQAM system cause a bandwidth efficiency loss of $\frac{1}{N+1}$ [10]. Hence, for a spreading length of 64, the loss in bandwidth efficiency is 1.54%. Taking into account this loss for the FBMC/OQAM system and all the overheads due to channel estimation, the theoretical bit rates that can be achieved with the standard and massive MIMO systems in the 1000 m vertically configured UAC are given in Table I. The 2×100 and 4×100 FBMC/OQAM systems achieve around 46% and 48% higher bit rate respectively than similar configuration OFDM systems. Compared to the N_t×12 standard MIMO systems, more than 50% increase in bit rate is achieved with the N_t×100 massive MIMO systems for the same channel.

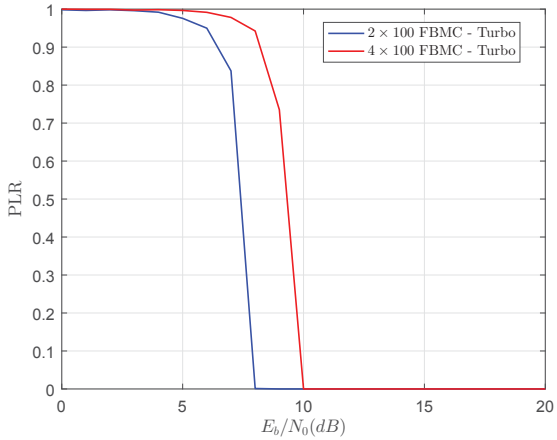

Fig. 4. PLR for transmission of 480p compressed video using 2×100 and 4×100 FBMC/OQAM systems

C. Video Evaluation

Our application targets real-time video which is captured by a camera, compressed using a suitable video compression standard and then transmitted over the error-prone channel. For the video transmission part, we consider the 2×100 and 4×100 Turbo-coded FBMC/OQAM systems since they achieve a higher bit rate and better error performance than the OFDM systems. H.264/AVC is chosen for video compression instead of High Efficiency Video Coding (HEVC) although the latter provides a better video quality for the same bit rate. HEVC has more computational overheads than H.264/AVC and has a lower error resilience due to the increase in the temporal dependency [17]. An uncompressed 480p (854×480) video with a frame rate of 30 fps and duration 12 s is compressed down to 130 kbps and 240 kbps for the 2×100 and 4×100 FBMC/OQAM systems respectively. The total number of frames in the video is 365. For low bit rate video coding, it is likely that a whole frame is encoded within a single packet and a single bit error in that packet will cause the entire frame to be lost [18], impacting severely on other frames within the group of pictures (GOP). Hence, an intra-period of 8 was chosen to provide increased error resilience. However, if the period is too small the target bit rate becomes difficult to achieve. The maximum packet length was set to 800 bytes and the number of reference frames was set to 6 to ensure a good compression efficiency.

1) Calculated Frame Rate: The number of bits per frame varies in the video sequence with the *I*-frames consisting of more bits than others. Hence an average number of bits per frame is used to compute the frame rate of the encoded video streams. The H.264/AVC videos compressed at 130 kbps and 240 kbps have an average number of bits per frame of 4,324 and 8,024 respectively. Considering the maximum achievable bit rates in Table I, the calculated frame rates for the 2×N_r and 4×N_r FBMC/OQAM systems are 30.76 fps and 30.16 fps respectively. Hence, real-time video transmission is

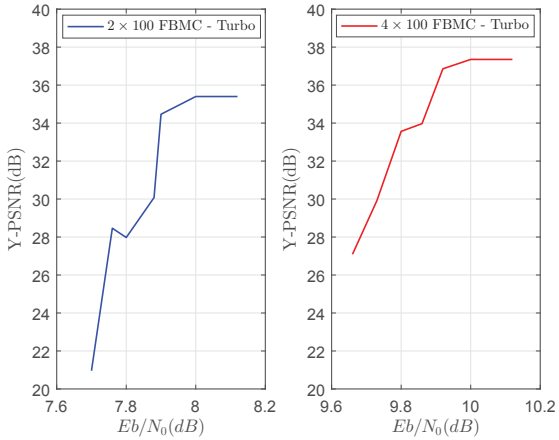

Fig. 5. PSNR versus E_b/N_0 for received video streams

theoretically possible with both systems.

2) Packet Loss Rate (PLR): Fig. 4 shows the PLR for the systems under investigation. The H.264/AVC bitstreams are encoded in 867 and 1008 video packets for the 2×100 and 4×100 systems respectively. The E_b/N_0 values that are required to achieve negligible bit errors and hence packet loss are 8 dB and 10 dB for the 2×100 and 4×100 systems respectively.

3) Video Quality: We evaluate the video quality in terms of Peak Signal-to-Noise Ratio (PSNR). Only the Y-component is considered since the human eye is more sensitive to luminance than chrominance. We consider the frame copy error concealment technique which works by copying the pixels located at the same spatial position from the previous frame in order to conceal the corrupted part of the frame. This method may be very effective if there is little motion from one frame to the next. Fig. 5 shows the PSNR plot between the raw 480p video and the received H.264/AVC video streams. For each system, the packet loss rate varies between 0 and 25%. Higher values for packet loss were not considered since the video streams became practically impossible to decode. With increasing E_b/N_0 values, it is observed that the video quality for each system has a general tendency to increase as the number of packet loss decreases. Assuming no packet loss, the 4×100 FBMC/OQAM system achieves a higher PSNR value (better video quality) than the 2×100 system.

V. Conclusion

FBMC/OQAM achieves a higher bit rate than OFDM due to the absence of a CP, making it attractive for underwater wireless video transmission. However, conventional FBMC/OQAM systems suffer from intrinsic imaginary interference. By spreading the symbols in time (or frequency), this interference can be eliminated and complex orthogonality restored without any increase in complexity. This enables the application of FBMC/OQAM to MIMO and the use of pilot-based channel estimation as in OFDM. The use of massive MIMO reception increases the reliability of the communication link, allowing higher order modulation schemes to be used with higher FEC code rates. This allows a higher bit rate to be achieved, promoting real-time video transmission. In this work, the bit rates obtained over the long distance acoustic link are sufficiently high to achieve an acceptable video quality which conveys useful information in real-time to the user.

References

[1] J. Ribas *et al.*, "Underwater wireless video transmission for supervisory control and inspection using acoustic OFDM," in *OCEANS 2010*, Sep. 2010, pp. 1–9.

[2] L. D. Vall *et al.*, "Towards underwater video transmission," in *Proceedings of the Sixth ACM International Workshop on Underwater Networks*. ACM, 2011, p. 4.

[3] B. Li *et al.*, "MIMO-OFDM for high-rate underwater acoustic communications," *IEEE Journal of Oceanic Engineering*, vol. 34, no. 4, pp. 634–644, Oct. 2009.

[4] E. V. Zorita and M. Stojanovic, "Space-frequency block coding for underwater acoustic communications," *IEEE Journal of Oceanic Engineering*, vol. 40, no. 2, pp. 303–314, Apr. 2015.

[5] A. Aminjavaheri and B. Farhang-Boroujeny, "UWA massive MIMO communications," in *OCEANS 2015 - MTS/IEEE Washington*, Oct 2015, pp. 1–6.

[6] P. Amini *et al.*, "Filterbank multicarrier communications for underwater acoustic channels," *Oceanic Engineering, IEEE Journal of*, vol. 40, no. 1, pp. 115–130, 2015.

[7] J. Gomes and M. Stojanovic, "Performance analysis of filtered multitone modulation systems for underwater communication," in *OCEANS 2009, MTS/IEEE Biloxi-Marine Technology for Our Future: Global and Local Challenges*. IEEE, 2009, pp. 1–9.

[8] A. Aminjavaheri *et al.*, "Frequency spreading Doppler scaling compensation in underwater acoustic multicarrier communications," in *Communications (ICC), 2015 IEEE International Conference on*, Jun. 2015, pp. 2774–2779.

[9] X. Zhao and D. Pompili, "AMMCA: Acoustic massive MIMO with carrier aggregation to boost the underwater communication data rate," in *Proceedings of the 10th International Conference on Underwater Networks & Systems*. ACM, 2015, p. 5.

[10] R. Nissel and M. Rupp, "Enabling low-complexity mimo in FBMC-OQAM," in *2016 IEEE Globecom Workshops (GC Wkshps)*, Dec 2016, pp. 1–6.

[11] H. Esmaiel and D. Jiang, "Review article: Multicarrier communication for underwater acoustic channel," *Int'l J. of Communications, Network and System Sciences*, vol. 6, no. 08, p. 361, 2013.

[12] M. C. Domingo, "Overview of channel models for underwater wireless communication networks," *Physical Communication*, vol. 1, no. 3, pp. 163–182, 2008.

[13] M. Stojanovic and J. Preisig, "Underwater acoustic communication channels: Propagation models and statistical characterization," *IEEE Communications Magazine*, vol. 47, no. 1, pp. 84–89, Jan. 2009.

[14] M. Stojanovic, "Underwater acoustic communications: Design considerations on the physical layer," in *Wireless on Demand Network Systems and Services, 2008. WONS 2008. Fifth Annual Conference on*. IEEE, 2008, pp. 1–10.

[15] F. X. Socheleau *et al.*, "A maximum entropy framework for statistical modeling of underwater acoustic communication channels," in *Proc. OCEANS 2010 IEEE - Sydney*, May 2010, pp. 1–7.

[16] M. Stojanovic, "MIMO OFDM over underwater acoustic channels," in *Proc. Systems and Computers 2009 Conf. Record of the Forty-Third Asilomar Conf. Signals*, Nov. 2009, pp. 605–609.

[17] A. Aldahdooh *et al.*, "Spatio-temporal error concealment technique for high order multiple description coding schemes including subjective assessment," in *2016 Eighth International Conference on Quality of Multimedia Experience (QoMEX)*, June 2016, pp. 1–6.

[18] A. M. Demirtas *et al.*, "Performance of H.264 with isolated bit error: Packet decode or discard?" in *2011 18th IEEE International Conference on Image Processing*, Sept 2011, pp. 949–952.